



Self-diffusion of pure and mixed gases in mixed-linker zeolitic imidazolate framework-7-8 by high field diffusion NMR

Samuel Berens^a, Febrian Hillman^b, Hae-Kwon Jeong^b, Sergey Vasenkov^{a,*}

^a Department of Chemical Engineering, University of Florida, Gainesville, FL, 32611, USA

^b Artie McFerrin Department of Chemical Engineering, Texas A&M University, College Station, TX, 77843, USA

ARTICLE INFO

Keywords:

MOF
ZIF
Diffusion
PFG NMR
Gas separation

ABSTRACT

Self-diffusion of pure gases including carbon dioxide, methane, ethylene, ethane, and xenon as well as selected two-component mixtures was studied in hybrid zeolitic imidazolate framework-7-8 (ZIF-7-8) crystals using pulsed field gradient (PFG) NMR. This material was formed by mixing 2-methylimidazolate (ZIF-8 linker) and bulkier benzimidazolate (ZIF-7 linker) in the same framework. The intracrystalline diffusion data measured in mixed-linker ZIF-7-8 was compared with the corresponding data in the parent ZIF-8 material. It was found that under the same or comparable experimental conditions the intracrystalline gas diffusion was always slower in ZIF-7-8 than in ZIF-8. This observation is consistent with the expected lower pore aperture size in ZIF-7-8 than in ZIF-8. At the same time, the ethane/ethylene diffusion selectivity was found to be similar in both ZIFs. It was also observed that for the pure studied gases larger than carbon dioxide the diffusivity ratios in ZIF-8 and ZIF-7-8 do not increase with increasing gas size at all loading pressures used. All these data are attributed to greater framework flexibility effects in ZIF-7-8 than ZIF-8. Such effects manifest themselves in a distortion and/or increase in the aperture size in the presence of large sorbates due to linker flexibility.

1. Introduction

Zeolitic imidazolate frameworks (ZIFs) are a subtype of metal organic frameworks (MOFs) which exhibit zeolite-like framework topologies [1]. ZIFs have been recognized for their ability to adsorb large quantities of gases as well as act as molecular sieves in the same manner as traditional aluminosilicates [2–9]. Mass transfer within ZIFs is limited by pore aperture sizes which can be commensurate to the size of molecules diffusing within the pores [2,4,5]. This makes ZIFs excellent candidates for separations applications in which similarly sized sorbates are sieved by a ZIF whose pore aperture size is comparable with the sorbate sizes.

Diffusion studies identifying and evaluating such potential for separations have been performed for a variety of sorbates in ZIF-8, the most well-studied ZIF, which is composed of Zn²⁺ metal ions and 2-methylimidazolate (mIm) linkers [1]. The separation potential related to diffusion can be quantified using a diffusion selectivity, i.e. diffusivity ratios under the same or similar conditions. CO₂ and CH₄ mixtures exhibit a notable diffusion selectivity in ZIF-8 owing to the larger kinetic diameter of CH₄ [8,10,11]. Larger hydrocarbons such as ethane and ethylene have been also found to have significant diffusion selectivity in ZIF-8 [4,12,13]. An even better diffusion selectivity than for

ethane/ethylene was observed for propane/propylene in ZIF-8 [14]. Apart from gases, ZIF-8 also has the capabilities to separate liquid compounds such as methanol/ethanol mixtures [15].

Despite the narrow crystallographic aperture size of the six-membered rings in ZIF-8 (~3.4 Å) [5], molecules with larger kinetic diameters such as propylene and propane are still able to enter and diffuse through the ZIF-8 framework [9]. This observation can be explained by the framework flexibility of the ZIF framework, which might result in the ability of the imidazolate linkers to “swing” to a greater degree in the presence of an adsorbed species. Framework flexibility effects can also explain the phenomenon in which species such as CH₄ diffuse faster at higher concentrations within ZIF-8; as the species deforms the framework, it can cause pore windows to open to a greater extent thereby increasing diffusivity for adsorbed molecules [16–19]. These flexibility effects have been further explored and validated for other sorbates such as ethane, ethylene, and Xe [20,21].

While other ZIFs with similar structures such as ZIF-11 and ZIF-90 have also been studied extensively for their sorption/diffusion properties [15,22], a more recent class of ZIFs whose sorbate diffusion properties have not yet been well investigated are mixed-linker ZIFs. These ZIFs utilize a combination of two different linkers to achieve intermediate properties of the ZIFs formed by either of the two parent

* Corresponding author.

E-mail address: svasenkov@che.ufl.edu (S. Vasenkov).

linkers [23–29]. A promising mixed-linker ZIF, ZIF-7-8, has been identified as a good potential candidate for optimized molecular sieving owing to the pore window tunability by mixing mIm (ZIF-8 linker) with bulkier benzimidazole (bIm, ZIF-7 linker) [24,25]. Our initial diffusion study performed in ZIF-7-8 by pulsed field gradient (PFG) NMR for a single sorbate (ethane) was recently reported [30]. Ethane self-diffusivity was found to vary significantly between individual ZIF-7-8 crystals as observed by PFG NMR in combination with single crystal IR microscopy, a powerful complimentary technique used in this study by our collaborators. In the present work, we expand the initial PFG NMR diffusion study of ethane in ZIF-7-8 to other sorbates including ethylene, CO₂, and CH₄. These sorbates were chosen for the industrially relevant and challenging processes of separating ethane/ethylene and CO₂/CH₄. Utilizing high magnetic field strengths (14 and 17.6 T) as well as large magnetic field gradients (up to 25 Tm⁻¹), we evaluate the ability of ZIF-7-8 to change the gas self-diffusivity in comparison to the parent ZIF-8 material and alter diffusion selectivity for the studied sorbates. Furthermore, we report mixed gas diffusion studies to determine the effect of co-adsorption of sorbates on diffusion selectivity and to evaluate the role of the framework flexibility of ZIF-7-8 in sorbate diffusion.

2. Experimental

2.1. Materials

Zinc nitrate hexahydrate (Zn(NO₃)₂·6H₂O, 98%, hereafter ZnN), 2-methylimidazole (C₄H₅N₂, 97%, hereafter mIm), benzimidazole (C₇H₆N₂, 98%, hereafter bIm), and sodium formate (HCOONa, 99%) were obtained from Sigma-Aldrich. Methanol (99.8%) and dimethylformamide (99.8%) were purchased from Alfa Aesar. All materials were used without any further purification. Single ¹³C-enriched ethane (C₂H₆), double ¹³C-enriched ethylene (C₂H₄), ¹³C carbon dioxide (CO₂), ¹³C methane (CH₄), and ¹²⁹Xe were selected as sorbates for diffusion studies in ZIF-8 and ZIF-7-8. All sorbates had > 99% isotopic purity (Sigma-Aldrich).

2.2. Synthesis of ZIF-8 and ZIF-7-8 and standard characterization

For synthesis of ZIF-8 crystals, a solution of 1.13 mmol of ZnN dissolved in 20 mL of methanol was poured to a solution of 1.01 mmol of mIm in 20 mL of methanol while continuously stirred for 1 min. The mixed solution was then transferred to a Teflon-lined steel autoclave to be reacted for 24 h at 50 °C in an oven. For ZIF-7-8, a solution of 3.34 mmol of ZnN in 20 mL of dimethylformamide was poured to a solution of 4.67 mmol of mIm, 0.35 mmol of bIm, and 1.66 mmol of sodium formate in 20 mL of methanol, and allowed to continuously stir for 1 min. The resulting solution was transferred to a Teflon-lined steel autoclave and placed in an oven for 2 h at 95 °C. For both ZIF-8 and ZIF-7-8, after the reaction in oven, the solution was cooled at room temperature for 2 h before opening the autoclave to collect the precipitates. The cooled solutions were then centrifuged at 8000 rpm for 10 min to obtain the powders. To wash the crystals, they were dispersed in 30 mL of methanol followed by centrifugation (8000 rpm for 10 min) for three times cycle. The washed ZIF-8 and ZIF-7-8 crystals were dried at 120 °C for 2 h prior to further characterization. The scanning electron microscopy (SEM) images of the ZIF-8 and ZIF-7-8 crystals as shown in Fig. S1 were obtained using JEOL JSM-7500F operating at acceleration voltage of 5 keV with working distance of 15 mm. The average crystal sizes of ZIF-8 and ZIF-7-8 were determined by averaging the width of 10 crystals observed by SEM. ZIF-8 and ZIF-7-8 samples had comparable spherical crystal diameters of 18 μm and 13 μm, respectively. Room temperature X-ray diffraction (XRD) analyses were performed to determine the crystal structure of the obtained ZIF-8 and ZIF-7-8 as shown in Fig. S2. Rigaku Miniflex II was used for XRD characterization using Cu-Kα radiation (λ = 1.5406 Å), scanned with step size of 0.02°. Ethane

and ethylene adsorption isotherms were performed on ZIF-8 and ZIF-7-8 on an ASAP 2010 (Micrometrics) (Fig. S3). ZIF-8 isotherms of the C₂ species match well with previously published isotherms [4].

2.3. NMR sample preparation

NMR diffusion studies were performed for two sorbate loadings corresponding to the sorbate loading pressures of around 7.8 and 0.8 bar. The samples were prepared by loading around 60 mg of ZIF sample into an NMR tube and degassing overnight (~10 h) in a custom-made vacuum system at 383 K and 0.080 mbar. Once the samples were made sorbate free via degassing and cooled down to room temperature, they were cryogenically loaded with a calculated amount of the desired gas necessary to achieve a pressure of around 8 or 0.8 bar in the gas volume of a sealed sample tube. These calculations were based on the adsorption isotherms of ZIF-7-8 (Fig. S3) or ZIF-8 [31,32] and known free gas volume of the tube. Once the gas was cryogenically transferred into the tubes using liquid nitrogen, the tubes were flame-sealed, separated from the vacuum system, and kept for at least 12 h at 296 ± 1 K before NMR studies to ensure that the sorption equilibrium was reached.

In addition to diffusion of pure gases, diffusion of the following binary mixtures was investigated in ZIF-7-8: C₂H₆/C₂H₄, CO₂/CH₄, and CO₂/C₂H₆. The equimolar gas mixtures were cryogenically transferred into NMR sample tube using the same procedure as with the single sorbate samples. Similarly, the mixed gas samples were flame sealed upon loading with total loading pressures around 8.2 bar at 296 ± 1 K.

Pressure in the gas phase of NMR samples with ZIFs was obtained by comparing NMR signal intensities measured for the gas phase of these samples with the corresponding signal in the reference samples containing only gas (no porous material added) at a known pressure. Concentrations inside the ZIF beds were calculated through a mass balance taking into account the known mass of the gas cryogenically added to the sample tubes. Concentrations matched adsorption isotherms for C₂ species in ZIF-7-8 and ZIF-8 as seen in Fig. S3.

2.4. PFG NMR measurements

¹³C and ¹²⁹Xe NMR measurements were performed on a 51 mm bore 14 T Avance III 600 MHz spectrometer (Bruker Biospin) and an 89 mm bore 17.6 T Avance III HD 750 MHz spectrometer. ¹³C PFG NMR was used for measurements of hydrocarbon diffusion instead of more traditional ¹H PFG NMR because of our previous observations of much longer T₂ NMR times of ¹³C than ¹H of hydrocarbons confined in ZIFs [22,30]. Only ¹²⁹Xe NMR measurements as well as a few selected ¹³C NMR measurements were performed at 17.6 T. These selected measurements were done to verify the results obtain at 14 T in order to confirm the absence of any measurement artifacts under our experimental conditions. Under the conditions of our ¹³C NMR measurements at 14 and 17.6 T the resonance frequencies were equal to 150.1 and 188.6 MHz, respectively. ¹²⁹Xe NMR measurements were performed at a resonance frequency of 208.6 MHz at 17.6 T. For each studied sorbate an NMR spectrum consisted of a single line. The following chemical shifts were observed: C₂H₆ (6 ppm), C₂H₄ (122 ppm), CO₂ (128 ppm), CH₄ (-8 ppm), and Xe (156 ppm in ZIF-7-8 and 152 ppm in ZIF-8). ¹³C and ¹²⁹Xe NMR chemical shifts are referenced to 40% 1,4-dioxane in benzene-d₆ at 67 ppm and gas phase Xe at 0 ppm, respectively. Fig. S4 displays representative NMR spectra of all species studied adsorbed in ZIF-7-8 at around 8 bar.

Diffusion measurements were performed using a 13-interval PFG NMR pulse sequence with bipolar gradients and an added longitudinal eddy-current delay of ~6 ms [33–35]. Diffusivities (D) were derived from the signal attenuation (Y) which measures NMR signal magnitude, i.e. area of NMR lines (S) as a function of gradient strength (g) and can be written as:

$$\psi = \frac{S(g)}{S(g \approx 0)} = \exp\left(-\frac{\langle r^2(t) \rangle}{6} q^2\right) = \exp(-q^2 D t) \quad (1)$$

where $q = 2\gamma g \delta$, γ is the gyromagnetic ratio, g is the gradient strength, δ is the effective gradient pulse length, t is diffusion time, and $\langle r^2(t) \rangle$ denotes the mean square displacements (MSD). MSD is related to D and t through the Einstein relation:

$$\langle r^2(t) \rangle = 6Dt \quad (2)$$

Bipolar, sine and trapezoidal-shaped magnetic field gradients were generated using a *Diff30* diffusion probe (Bruker Biospin) at 14 T and a *Diff50* diffusion probe (Bruker Biospin) at 17.6 T. Gradient pulse durations (δ) ranged from 1.5 to 3.5 ms for both probes and had a maximum amplitude around 11 T/m for the *Diff30* and 20 T/m for the *Diff50*. Typical PFG NMR experiments had between 256 and 1024 scans for each gradient step, total experimental times between 1 and 5 h, and repetition delays between 1 and 4 s (set at minimum 1.5 times greater than the T_1 relaxation time). NMR spectra were measured using a single radiofrequency pulse sequence before and after diffusion measurements to confirm the absence of any changes in sorbate concentration over the time of the experiments (see Fig. S4 for representative spectra of all sorbates).

Longitudinal (T_1) relaxation measurements were performed using the standard inversion recovery sequence. Transverse (T_2) relaxation measurements were done using the 13-interval PFG NMR sequence by changing the time intervals during which the T_2 NMR relaxation takes place and keeping all other intervals constant as done in previous studies [36]. In all samples, there was no observed distribution of T_1 or T_2 relaxation times for the adsorbed sorbates. T_1 and T_2 relaxation times are shown in Tables S1 and S2. All NMR measurements were performed at 296 ± 1 K.

3. Results and discussion

Figs. 1 and 2 show ^{13}C PFG NMR attenuation curves for the diffusion of four gases in ZIF-7-8 at the high and low loadings corresponding to the loading pressure of around 7.8 and 0.8 bar at 296 ± 1 K,

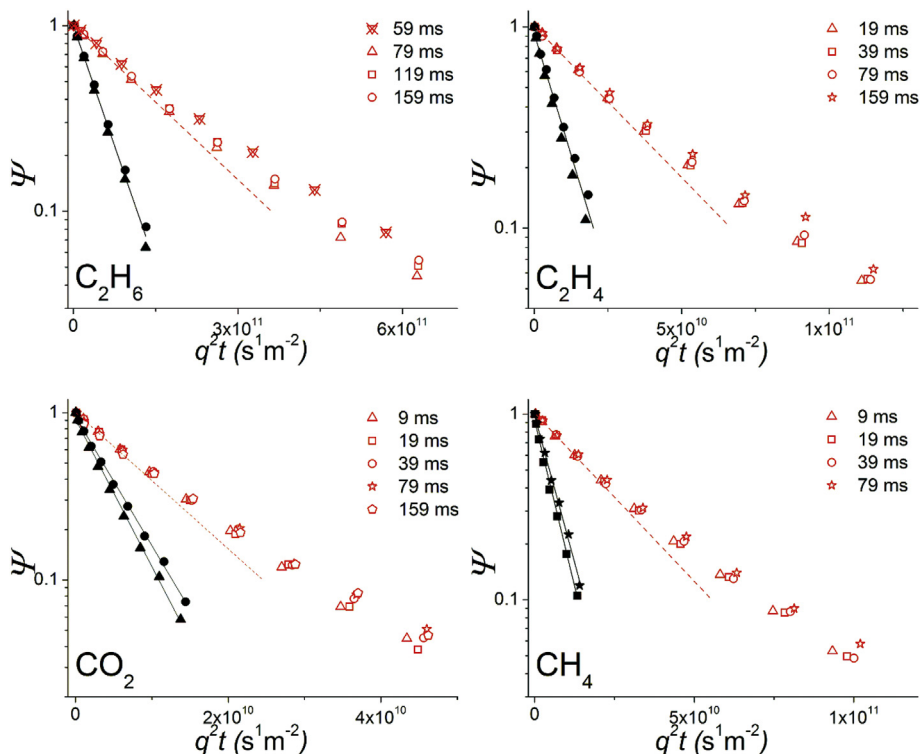


Fig. 1. ^{13}C PFG NMR attenuation curves at high sorbate loadings corresponding to a loading pressure of 7.8 ± 0.8 bar at 296 K for various diffusion times (see figure legend) measured for C_2H_6 [30], C_2H_4 , CO_2 , and CH_4 in ZIF-7-8 (empty, red symbols) and ZIF-8 (filled, black symbols). The solid lines for the ZIF-8 data represent a monoexponential fit (Eq. (1)) while the dashed red lines are the “effective” monoexponential fits based on the initial 30% of the signal attenuation in ZIF-7-8 and extrapolated to the signal attenuation values around 0.1. Crossed symbols correspond to the measurements at 17.6 T. All other symbols correspond to the measurements at 14 T. (For interpretation of the references to colour in this figure legend, the reader is referred to the Web version of this article.)

respectively. Ethane attenuation curves were previously reported in Ref. [30] and are shown in Figs. 1 and 2 for comparison to other sorbates. Also shown for comparison are the corresponding measured attenuation curves in ZIF-8, which was used as a reference material. It is important to note that ^{13}C T_2 NMR relaxation times of small gas molecules in ZIF-7, another reference material for ZIF-7-8, were found to be too small for meaningful PFG NMR measurements [30]. PFG NMR measurements in ZIF-7-8 and ZIF-8 were performed for different diffusion times shown in the figures. It is seen that in contrast to the monoexponential attenuation behavior in agreement with Eq. (1) observed for ZIF-8 (linear in the semilogarithmic presentation of Figs. 1 and 2), all the attenuation curves measured for ZIF-7-8 exhibit deviations from a monoexponential decay. The absence of any measurement artifacts in the attenuation data at 14 T was confirmed by the measurements of the same sample under the same conditions at 17.6 T (see data for C_2H_6 in Fig. 1). Coinciding attenuation curves measured for C_2H_6 at the different field strength provide such confirmation. Despite the deviations from the monoexponential behavior, the attenuation curves measured for the same ZIF-7-8 sample at different diffusion times coincide, within uncertainty, in the presentation of Figs. 1 and 2. The results of the recently published study of ethane diffusion in the same ZIF-7-8 sample as that used in the current work show that the observed deviations from the monoexponential behavior originate from the existence of differences between sorbate diffusivities in different ZIF-7-8 crystals of the sample [30]. In particular, single crystal IR microscopy measurements of the ethane transport diffusivities reported in Ref. [30] were found to vary significantly (up to a factor of 4.4) between randomly selected individual ZIF-7-8 crystals, thereby indicating there is indeed heterogeneity in transport properties between individual crystals. This heterogeneity was attributed to the difference in the fractions of mIm and bIm linkers observed for different ZIF-7-8 crystals from the studied sample by single crystal IR microscopy. The deviations from monoexponential attenuation in Figs. 1 and 2 confirm that the distribution of self-diffusivities between crystals exists for all gaseous sorbates studied.

An effective (average) diffusivity in the samples exhibiting distribution over diffusion coefficients can be obtained by fitting the initial

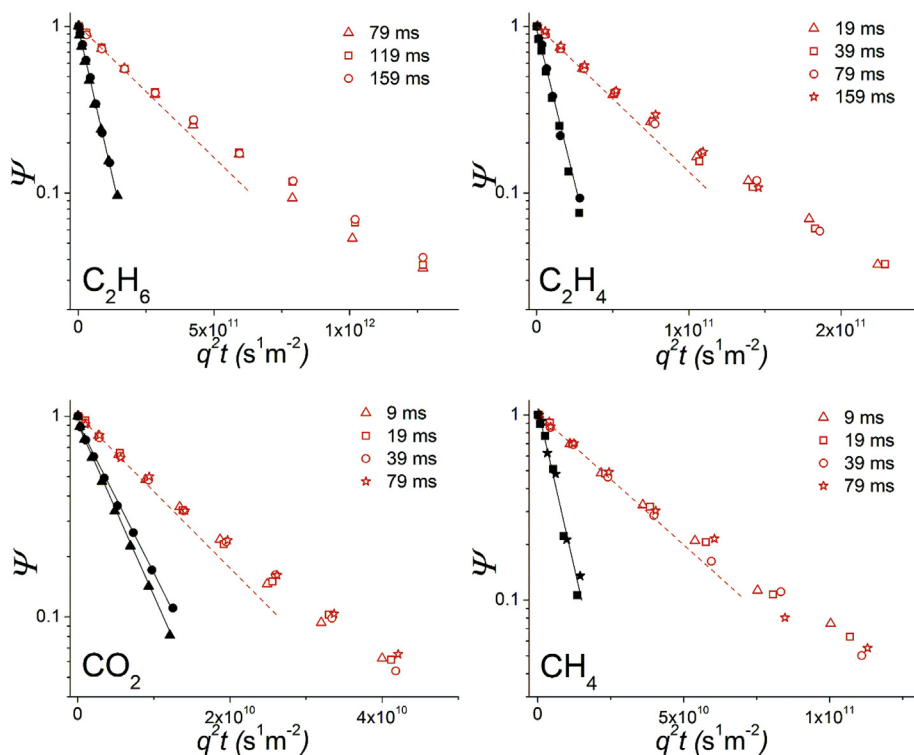


Fig. 2. ^{13}C PFG NMR attenuation curves at low sorbate loadings (loading pressure above ZIF bed of 0.8 ± 0.08 bar) for various diffusion times (see figure legend) of ^{13}C labelled C_2H_6 [30], C_2H_4 , CO_2 , and CH_4 gas at 296 K in ZIF-7-8 (open symbols) and ZIF-8 (filled symbols). The solid lines for the ZIF-8 data represent a monoexponential fit (Eq. (1)) while the dashed red lines are the “effective” monoexponential fits based on the initial 30% of the signal attenuation in ZIF-7-8 and extrapolated to the signal attenuation values around 0.1. All data were measured on a 14 T spectrometer. (For interpretation of the references to colour in this figure legend, the reader is referred to the Web version of this article.)

Table 1

Effective diffusivities and the corresponding ranges of root mean square displacement (RMSD) values measured by PFG NMR for pure gases in ZIF-7-8 at 296 K.

Material	Gas	Pressure above ZIF Bed (bar)	Concentration of Gas in ZIF (mmol/g)	$D_{\text{eff}} \times 10^{-11}$ (m^2s^{-1})	$D_{\text{eff}}/p \times 10^{-11}$ (m^2s^{-1} mmol/(g bar)) ^a	RMSD Range (μm)
ZIF-7-8	C_2H_6	7.9 ± 0.8	4.4 ± 1.1	0.64 ± 0.10	0.36	1.7 to 2.5
ZIF-7-8	C_2H_6	2.7 ± 0.3	2.9 ± 0.6	0.51 ± 0.08	0.56	1.3 to 2.2
ZIF-7-8	C_2H_6	0.78 ± 0.08	1.5 ± 0.3	0.36 ± 0.05	0.68	1.3 to 1.9
ZIF-7-8	C_2H_6	0.28 ± 0.03	1.1 ± 0.3	0.36 ± 0.05	1.4	1.3 to 1.9
ZIF-7-8	C_2H_4	8.1 ± 0.8	3.9 ± 0.8	3.5 ± 0.5	1.7	2.0 to 5.8
ZIF-7-8	C_2H_4	0.88 ± 0.13	0.88 ± 0.18	2.0 ± 0.3	2.0	1.5 to 4.4
ZIF-7-8	CO_2	7.6 ± 0.8	5.5 ± 1.1	9.1 ± 1.4	6.6	2.2 to 9.3
ZIF-7-8	CO_2	0.82 ± 0.12	0.48 ± 0.10	8.8 ± 1.3	5.1	2.2 to 6.5
ZIF-7-8	CH_4	7.6 ± 0.8	1.0 ± 0.2	4.2 ± 0.6	0.55	1.5 to 4.5
ZIF-7-8	CH_4	0.81 ± 0.12	0.15 ± 0.03	3.3 ± 0.5	0.60	1.3 to 4.0

^a All D_{eff}/p values have an uncertainty of 40%.

part of the PFG NMR attenuation curves by Eq. (1) [37]. Table 1 shows such effective diffusivities in ZIF-7-8 that were obtained by fitting Eq. (1) to the attenuation data in Figs. 1 and 2 with amplitudes of Ψ between around 1.0 and 0.7. The slopes corresponding to the effective diffusivities are shown by red dashed lines in Figs. 1 and 2. Table 1 also shows the corresponding ranges of the root MSD values obtained using the Einstein relation (Eq. (2)) for the diffusion times used in the measurements. It was observed that in all cases these root MSD values were significantly smaller than the mean size of ZIF-7-8 crystals ($\sim 13 \mu\text{m}$). Hence, any influence of the external crystal surface on the attenuation curves measured in ZIF-7-8 can be expected to be negligibly small [37]. This expectation is confirmed by the observed time independence of the effective diffusivities in ZIF-7-8 and by the coincidence of the corresponding attenuation curves for different diffusion times in the measured range (Figs. 1 and 2).

The results of fitting the attenuation curves for ZIF-8 in Figs. 1 and 2 using Eq. (1) at the smallest diffusion time along with the corresponding root MSD values are presented in Table S1. The smallest diffusion time data were used here and later to minimize any effects at the external crystal surface on the reported intra-ZIF diffusivities. Indeed, it is seen in Figs. 1 and 2 that for the smaller sorbates exhibiting faster diffusion in ZIF-8 there is some weak dependence of the

attenuation curves on diffusion time. Such dependence is attributed to the contribution of the effects at the external crystal surface because for faster diffusing sorbates root MSD values become comparable with the average size of ZIF-8 crystals ($\sim 18 \mu\text{m}$). It was verified that the intracrystalline diffusivities measured for ZIF-8 in this work (Table S1) are in agreement, within uncertainty, with the previously published self-diffusivities measured by PFG NMR under the same or similar conditions [12,19,20]. Fig. 3 presents the ratios of the corresponding diffusivities in ZIF-8 and ZIF-7-8. It is seen in the figure that for each sorbate and loading pressure studied the self-diffusivity in ZIF-7-8 is much lower than that in ZIF-8, which is consistent with previously published permeation measurements [24]. The data in this figure will be discussed in more detail later.

In addition to diffusion of pure gases discussed above, diffusion of the following two-component gas mixtures was investigated in ZIF-7-8 by ^{13}C PFG NMR: $\text{C}_2\text{H}_4/\text{C}_2\text{H}_6$, CO_2/CH_4 and $\text{CO}_2/\text{C}_2\text{H}_6$. The sorbate loadings corresponded to sorption equilibrium at the total loading pressure of around 8 bar at 296 ± 1 K and equal or similar partial pressures of each sorbate. Figs S5, S6 and S7 present the PFG NMR attenuation curves for the mixed gas samples. Table 2 shows the effective diffusivities of each sorbate in the two-component mixtures. These diffusivities were obtained from the initial slopes of the

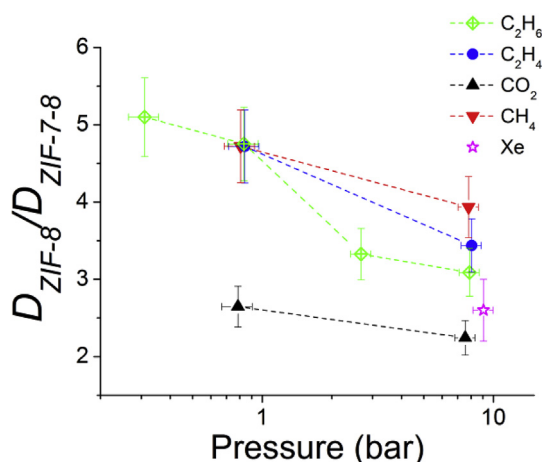


Fig. 3. Ratios of the sorbate self-diffusivities (D) in ZIF-8 to the effective self-diffusivities (D_{eff}) in ZIF-7-8 for C_2H_6 , C_2H_4 , CO_2 , CH_4 , and Xe at multiple sorbate loading pressures at 296 K.

attenuation curves as discussed above for the pure gases. Also shown in the table are the ranges of root MSD values calculated using Eq. (2).

The diffusion data in Tables 1 and 2 suggest that the diffusivity inside ZIF-7-8 crystals tends to increase with increasing total sorbate loading, especially when larger molecules like C_2H_6 (4.4 Å) [38,39] or C_2H_4 (4.2 Å) [38,39] are present in the sample. In particular, it was observed that the diffusivity of CO_2 in ZIF-7-8 is larger by a factor of around 1.4 when the sample is equilibrated with the $\text{CO}_2/\text{C}_2\text{H}_6$ mixture instead of pure CO_2 at a similar total loading pressure around 8 bar. For ZIF-7-8 loaded with pure ethane or ethylene the diffusivity is significantly larger when the loading pressure of the corresponding gas is larger. At the same time, for ZIF-7-8 loaded with pure CO_2 (3.3 Å) [39], the diffusivity is similar in the samples equilibrated with around 0.7 and 8 bar of CO_2 . Diffusivity increase with increasing sorbate loading was also previously reported for ZIF-8 [16–19], and attributed mostly to the framework flexibility of ZIF-8.

It is important to note that, according to the transition state theory (TST) applied in its simplest form to the process of a molecular passage through narrow apertures separating adjacent pores, the self-diffusivity in microporous solids is expected to be proportional to the ratio of the sorbate pressure in the gas phase surrounding microporous particles (p) and the intra-particle sorbate concentration (c) [40]. In a recent study, the concentration dependence of the corrected diffusivity of several gases in ZIF-8 was successfully explained by this simple approach [41]. In order to evaluate the applicability of this approach to the observed concentration dependence of the self-diffusivity in ZIF-7-8, the values of $D_{\text{eff}}c/p$ were calculated and presented in Tables 1 and 2 for the pure and mixed gases. According to the TST approach, such values for a particular sorbate should be concentration independent, even in the case of mixed gas samples [42]. The data in the tables indicate that within a large experimental uncertainty of these values (40%) they are the same for each particular gas at different loading pressures, for the exception of ethane at the highest loading pressures. In this case, the TST approach overpredicts the self-diffusivity increase with an increasing ethane loading. This can be explained by additional factors such as framework flexibility related effects or molecular crowding effects, which are not taken into account by the simple TST approach discussed above. Qualitatively the same conclusion can also be made for the gas self-diffusion in the reference ZIF-8 material based on the comparison of the Dc/p values in Table S1 for the same gas type. Hence, the diffusivity increase with increasing loading pressure observed in the current work can be explained using the TST approach.

Most remarkably, the data in Fig. 3 show that for the sorbates larger than CO_2 at any given loading pressure used for the measurements of more than a single sorbate type there is no increase in the diffusivity

Table 2
Effective diffusivities and the corresponding ranges of root mean square displacement (RMSD) values measured by PFG NMR for gas mixtures in ZIF-7-8 at 296 K.

Mixed Gas Samples in ZIF-7-8	Total Pressure Above Particle Bed (bar)		Partial Pressure Above Particle Bed (bar)		Total Concentration (mmol/g)	Partial Concentration (mmol/g)	$D_{\text{eff}}c/p \times 10^{-11}$ (m^2s^{-1} bar) ^a	$D_{\text{eff}}/p \times 10^{-11}$ (m^2s^{-1} bar) ^a	RMSD range (μm)
	8.2 ± 0.8	8.2 ± 0.8	4.2 ± 0.4	4.1 ± 0.4					
Ethane ($\text{C}_2\text{H}_6/\text{C}_2\text{H}_4$ mix)	8.2 ± 0.8	8.2 ± 0.8	4.2 ± 0.4	4.1 ± 0.4	3.2 ± 0.7	1.6 ± 0.3	0.71 ± 0.11	0.27	1.3 to 2.6
Ethylene ($\text{C}_2\text{H}_6/\text{C}_2\text{H}_4$ mix)	8.2 ± 0.8	8.2 ± 0.8	4.1 ± 0.4	4.1 ± 0.4	3.2 ± 0.7	1.6 ± 0.3	3.7 ± 0.6	1.4	1.4 to 5.9
CO_2 (CO_2/CH_4 mix)	7.7 ± 0.8	7.7 ± 0.8	3.9 ± 0.4	3.9 ± 0.4	3.5 ± 0.7	2.9 ± 0.6	9.0 ± 1.4	6.8	2.2 to 6.5
CH_4 (CO_2/CH_4 mix)	7.7 ± 0.8	7.7 ± 0.8	3.8 ± 0.4	3.8 ± 0.4	3.5 ± 0.7	0.60 ± 0.12	4.3 ± 0.6	0.68	1.5 to 4.5
CO_2 ($\text{CO}_2/\text{C}_2\text{H}_6$ mix)	8.6 ± 0.9	8.6 ± 0.9	4.5 ± 0.5	4.5 ± 0.5	3.6 ± 0.7	1.8 ± 0.4	13 ± 2	5.3	2.8 to 7.9
Ethane ($\text{CO}_2/\text{C}_2\text{H}_6$ mix)	8.6 ± 0.9	8.6 ± 0.9	4.2 ± 0.4	4.2 ± 0.4	3.6 ± 0.7	1.8 ± 0.4	0.61 ± 0.09	0.26	1.2 to 2.4

^a All $D_{\text{eff}}c/p$ values have an uncertainty of 40%. c and p represent partial concentration and partial pressure in the mixed gas sample.

Table 3

Single component and mixed gas effective diffusion selectivities in ZIF-7-8 and single component diffusion selectivities in ZIF-8 at 296 K.

Material	Loading Pressure (bar)	Single Component or Mixed Gas	CO ₂ /CH ₄ Diffusion Selectivity	C ₂ H ₄ /C ₂ H ₆ Diffusion Selectivity
ZIF-8	8	Single	1.2 ± 0.1	6.0 ± 0.6
ZIF-8	0.8	Single	1.5 ± 0.2	5.5 ± 0.6
ZIF-7-8	8	Single	2.2 ± 0.2	5.4 ± 0.5
ZIF-7-8	0.8	Single	2.7 ± 0.3	5.5 ± 0.6
ZIF-7-8	8	Mixed	2.1 ± 0.2	5.2 ± 0.5

ratio in ZIF-8 and ZIF-7-8 with increasing size of gas molecules. Such an increase is expected for rigid apertures, which are smaller for ZIF-7-8 than for ZIF-8. Furthermore, complementary measurements of Xe diffusion in both ZIFs using ¹²⁹Xe PFG NMR (Fig. S8 and Table S3) show that for the large loading pressure around 8 bar the diffusivity ratio for Xe is comparable with that for CO₂, despite the fact that the kinetic diameter of CO₂ is much smaller than that of Xe (~4.1 Å) [39,43]. All these observations suggest a larger influence of the framework flexibility on diffusion in ZIF-7-8 than in ZIF-8, especially for larger sorbates (C₂H₆, C₂H₄, and Xe).

Further indication of an increased influence of the framework flexibility on diffusion in ZIF-7-8 relative to ZIF-8 can be seen in Table 3. This table shows diffusion selectivities, which are defined as the ratios of the diffusivities of single sorbates in a mixture or the corresponding ratios for pure gases in the same porous material: $S_{a/b} = D_a/D_b$. For each material, diffusion selectivities remain the same within uncertainty between high and low loadings for both sets of gases being compared. It is seen that for the smaller sorbates (CO₂ and CH₄) the diffusion selectivity is larger in ZIF-7-8 than in ZIF-8, which is consistent with slower diffusion and expected smaller aperture sizes in the former ZIF in comparison with the latter. At the same time, for the larger sorbates (C₂H₄ and C₂H₆) the diffusion selectivity is similar in both ZIFs. Clearly, a higher extent of the framework flexibility in ZIF-7-8 in comparison to ZIF-8 can explain our results. This explanation is consistent with the computational results by Krokadis et al. indicating that ZIF-7-8 framework is more flexible than ZIF-8 though its effective aperture size is smaller [44]. In general, linker segmental dynamics is dominated by the flip-flopping motion of the linker in ZIF-8 as demonstrated by ²H NMR [45].

4. Conclusions

A multinuclear PFG NMR technique was used to study microscale transport properties of a mixed-linker ZIF, ZIF-7-8, using multiple pure and mixed gases as probe molecules. The PFG NMR data reported here for ZIF-7-8 exhibits evidence of a distribution of diffusivities between ZIF-7-8 crystals in the studied sample, in agreement with the previously reported observation of such distribution for ethane diffusion using PFG NMR in combination with single-crystal IR microscopy. For each studied gas the effective (average) diffusivity in ZIF-7-8 was compared with the corresponding diffusivity in its parent material, ZIF-8. In all cases the measured self-diffusivities were found to be significantly lower in ZIF-7-8 than in ZIF-8. ZIF-7-8 was found to exhibit improved diffusion selectivity compared to ZIF-8 for CO₂/CH₄. It was attributed to the better sieving caused by the expected smaller pore aperture size in ZIF-7-8 than in ZIF-8. At the same time, similar diffusion selectivities were observed in both ZIFs for larger molecules (C₂H₄/C₂H₆). This observation was explained by framework flexibility effects, which manifest themselves in a distortion/increase of pore apertures when large sorbates are present inside ZIF-7-8. Although framework flexibility effects are also expected in the parent ZIF-8 material, these effects are more pronounced in ZIF-7-8, as demonstrated by the comparison of the diffusivity values and diffusion selectivities in both ZIFs

for different sorbate types and sorbate loadings.

Conflicts of interest

The authors have no competing interests to declare.

Acknowledgements

This work was supported by the National Science Foundation (NSF awards No. 1561347). A portion of this work was performed in the McKnight Brain Institute at the National High Magnetic Field Laboratory's AMRIS Facility, which is supported by NSF Cooperative Agreement Nos. DMR-1157490 and DMR-1644779 and the State of Florida. This work was supported in part by an NIH award S10FF031637, for magnetic resonance instrumentation. H.-K.J. acknowledges the financial support from the National Science Foundation (CMMI-1561897). This publication was made possible in part by NPRP grant # 8-001-2-001 from the Qatar National Research Fund (a member of Qatar Foundation). The findings achieved herein are solely the responsibility of the authors.

Appendix A. Supplementary data

Supplementary data to this article can be found online at <https://doi.org/10.1016/j.micromeso.2019.109603>.

References

- [1] K.S. Park, Z. Ni, A.P. Cote, J.Y. Choi, R. Huang, F.J. Uribe-Romo, H.K. Chae, M. O'Keeffe, O.M. Yaghi, Exceptional chemical and thermal stability of zeolitic imidazolate frameworks, *Proc. Natl. Acad. Sci. U.S.A.* 103 (2006) 10186–10191.
- [2] R. Banerjee, H. Furukawa, D. Britt, C. Knobler, M. O'Keeffe, O.M. Yaghi, Control of pore size and functionality in isorecticular zeolitic imidazolate frameworks and their carbon dioxide selective capture properties, *J. Am. Chem. Soc.* 131 (2009) 3875–3877.
- [3] R. Banerjee, A. Phan, B. Wang, C. Knobler, H. Furukawa, M. O'Keeffe, O.M. Yaghi, High-throughput synthesis of zeolitic imidazolate frameworks and application to CO₂ capture, *Science* 319 (2008) 939–943.
- [4] H. Bux, C. Chmelik, R. Krishna, J. Caro, Ethene/ethane separation by the MOF membrane ZIF-8: molecular correlation of permeation, adsorption, diffusion, *J. Membr. Sci.* 369 (2011) 284–289.
- [5] H. Bux, F. Liang, Y. Li, J. Cravillon, M. Wiebcke, J. Caro, Zeolitic imidazolate framework membrane with molecular sieving properties by microwave-assisted solvothermal synthesis, *J. Am. Chem. Soc.* 131 (2009) 16000–16001.
- [6] T. Chokbunpium, S. Fritzsche, C. Chmelik, J. Caro, W. Janke, S. Hannongbua, Gate opening, diffusion, and adsorption of CO₂ and N₂ mixtures in ZIF-8, *J. Phys. Chem. C* 120 (2016) 23458–23468.
- [7] Q. Song, S.K. Nataraj, M.V. Roussanova, J.C. Tan, D.J. Hughes, W. Li, P. Bourgoin, M.A. Alam, A.K. Cheetham, S.A. Al-Muhtaseb, E. Sivaniah, Zeolitic imidazolate framework (ZIF-8) based polymer nanocomposite membranes for gas separation, *Energy Environ. Sci.* 5 (2012) 8359.
- [8] S.R. Venna, M.A. Carreon, Highly permeable zeolite imidazolate framework-8 membranes for CO₂/CH₄ separation, *J. Am. Chem. Soc.* 132 (2010) 76–78.
- [9] C. Zhang, R.P. Lively, K. Zhang, J.R. Johnson, O. Karvan, W.J. Koros, Unexpected molecular sieving properties of zeolitic imidazolate framework-8, *J. Phys. Chem. Lett.* 3 (2012) 2130–2134.
- [10] C. Chmelik, J. van Baten, R. Krishna, Hindering effects in diffusion of CO₂/CH₄ mixtures in ZIF-8 crystals, *J. Membr. Sci.* 397–398 (2012) 87–91.
- [11] E. Pantatosaki, G. Megariotis, A.-K. Pusch, C. Chmelik, F. Stallmach, G.K. Papadopoulos, On the impact of sorbent mobility on the sorbed phase equilibria and dynamics: a study of methane and carbon dioxide within the zeolite imidazolate framework-8, *J. Phys. Chem. C* 116 (2011) 201–207.
- [12] C. Chmelik, D. Freude, H. Bux, J. Haase, Ethene/ethane mixture diffusion in the MOF sieve ZIF-8 studied by MAS PFG NMR diffusometry, *Microporous Mesoporous Mater.* 147 (2012) 135–141.
- [13] N. Dvoyashkina, D. Freude, S.S. Arzumanov, A.G. Stepanov, Monitoring the diffusivity of light hydrocarbons in a mixture by magic angle spinning pulsed field gradient NMR: methane/ethane/ethene in ZIF-8, *J. Phys. Chem. C* 121 (2017) 25372–25376.
- [14] H.T. Kwon, H.K. Jeong, In situ synthesis of thin zeolitic-imidazolate framework ZIF-8 membranes exhibiting exceptionally high propylene/propane separation, *J. Am. Chem. Soc.* 135 (2013) 10763–10768.
- [15] J.A. Gee, J. Chung, S. Nair, D.S. Sholl, Adsorption and diffusion of small alcohols in zeolitic imidazolate frameworks ZIF-8 and ZIF-90, *J. Phys. Chem. C* 117 (2013) 3169–3176.
- [16] D. Fairen-Jimenez, S.A. Moggach, M.T. Wharmby, P.A. Wright, S. Parsons, T. Duren, Opening the gate: framework flexibility in ZIF-8 explored by experiments

- and simulations, *J. Am. Chem. Soc.* 133 (2011) 8900–8902.
- [17] E. Haldoupis, T. Watanabe, S. Nair, D.S. Sholl, Quantifying large effects of framework flexibility on diffusion in MOFs: CH₄ and CO₂ in ZIF-8, *ChemPhysChem* 13 (2012) 3449–3452.
- [18] L. Hertag, H. Bux, J. Caro, C. Chmelik, T. Remsungnen, M. Knauth, S. Fritzsche, Diffusion of CH₄ and H₂ in ZIF-8, *J. Membr. Sci.* 377 (2011) 36–41.
- [19] A.-K. Pusch, T. Splith, L. Moschkowitz, S. Karmakar, R. Biniwale, M. Sant, G.B. Suffritti, P. Demontis, J. Cravillon, E. Pantatosaki, F. Stallmach, NMR studies of carbon dioxide and methane self-diffusion in ZIF-8 at elevated gas pressures, *Adsorption* 18 (2012) 359–366.
- [20] R. Mueller, V. Hariharan, C. Zhang, R. Lively, S. Vasenkov, Relationship between mixed and pure gas self-diffusion for ethane and ethene in ZIF-8/6FDA-DAM mixed-matrix membrane by pulsed field gradient NMR, *J. Membr. Sci.* 499 (2016) 12–19.
- [21] M.A. Springuel-Huet, A. Nossouf, F. Guenneau, A. Gedeon, Flexibility of ZIF-8 materials studied using ¹²⁹Xe NMR, *Chem. Commun.* 49 (2013) 7403–7405.
- [22] E.M. Forman, B.R. Pimentel, K.J. Ziegler, R.P. Lively, S. Vasenkov, Microscopic diffusion of pure and mixed methane and carbon dioxide in ZIF-11 by high field diffusion NMR, *Microporous Mesoporous Mater.* 248 (2017) 158–163.
- [23] K. Eum, K.C. Jayachandrababu, F. Rashidi, K. Zhang, J. Leisen, S. Graham, R.P. Lively, R.R. Chance, D.S. Sholl, C.W. Jones, S. Nair, Highly tunable molecular sieving and adsorption properties of mixed-linker zeolitic imidazolate frameworks, *J. Am. Chem. Soc.* 137 (2015) 4191–4197.
- [24] F. Hillman, J. Brito, H.K. Jeong, Rapid one-pot microwave synthesis of mixed-linker hybrid zeolitic-imidazolate framework membranes for tunable gas separations, *ACS Appl. Mater. Interfaces* 10 (2018) 5586–5593.
- [25] F. Hillman, J.M. Zimmerman, S.-M. Paek, M.R.A. Hamid, W.T. Lim, H.-K. Jeong, Rapid microwave-assisted synthesis of hybrid zeolitic-imidazolate frameworks with mixed metals and mixed linkers, *J. Mater. Chem.* 5 (2017) 6090–6099.
- [26] K.C. Jayachandrababu, D.S. Sholl, S. Nair, Structural and mechanistic differences in mixed-linker zeolitic imidazolate framework synthesis by solvent assisted linker exchange and de Novo routes, *J. Am. Chem. Soc.* 139 (2017) 5906–5915.
- [27] K.C. Jayachandrababu, R.J. Verploegh, J. Leisen, R.C. Nieuwendaal, D.S. Sholl, S. Nair, Structure elucidation of mixed-linker zeolitic imidazolate frameworks by solid-state (1)H CRAMPS NMR spectroscopy and computational modeling, *J. Am. Chem. Soc.* 138 (2016) 7325–7336.
- [28] J.-S. Qin, S. Yuan, Q. Wang, A. Alsalmeh, H.-C. Zhou, Mixed-linker strategy for the construction of multifunctional metal-organic frameworks, *J. Math. Chem. A* 5 (2017) 4280–4291.
- [29] J.A. Thompson, C.R. Blad, N.A. Brunelli, M.E. Lydon, R.P. Lively, C.W. Jones, S. Nair, Hybrid zeolitic imidazolate frameworks: controlling framework porosity and functionality by mixed-linker synthesis, *Chem. Mater.* 24 (2012) 1930–1936.
- [30] S. Berens, C. Chmelik, F. Hillman, J. Karger, H.K. Jeong, S. Vasenkov, Ethane diffusion in mixed linker zeolitic imidazolate framework-7-8 by pulsed field gradient NMR in combination with single crystal IR microscopy, *Phys. Chem. Chem. Phys.* 20 (2018) 23967–23975.
- [31] C. Chmelik, Characteristic features of molecular transport in MOF ZIF-8 as revealed by IR microimaging, *Microporous Mesoporous Mater.* 216 (2015) 138–145.
- [32] J. Perez-Pellitero, H. Amrouche, F.R. Siperstein, G. Pirngruber, C. Nieto-Draghi, G. Chaplais, A. Simon-Masseron, D. Bazer-Bachi, D. Peralta, N. Bats, Adsorption of CO₂, CH₄, and N₂ on zeolitic imidazolate frameworks: experiments and simulations, *Chemistry* 16 (2010) 1560–1571.
- [33] P. Galvosas, F. Stallmach, G. Seiffert, J. Kärger, U. Kaess, G. Majer, Generation and application of ultra-high-intensity magnetic field gradient pulses for NMR spectroscopy, *J. Magn. Reson.* 151 (2001) 260–268.
- [34] R.M. Cotts, M.J.R. Hoch, T. Sun, J.T. Markert, Pulsed field gradient stimulated echo methods for improved NMR diffusion measurements in heterogeneous systems, *J. Magn. Reson.* 83 (1989) 252–266.
- [35] S.J. Gibbs, C.S. Johnson, A pfg nmr experiment for accurate diffusion and flow studies in the presence of eddy currents, *J. Magn. Reson.* 93 (1991) 395–402.
- [36] E.M. Forman, B.R. Pimentel, K.J. Ziegler, R.P. Lively, S. Vasenkov, Microscopic diffusion of pure and mixed methane and carbon dioxide in ZIF-11 by high field diffusion NMR, *Microporous Mesoporous Mater.* 248 (2017) 158–163.
- [37] J. Kärger, D.M. Ruthven, D.N. Theodorou, *Diffusion in Nanoporous Materials 2 Volume Set* Wiley, 2012.
- [38] S. Aguado, G. Bergeret, C. Daniel, D. Farrusseng, Absolute molecular sieve separation of ethylene/ethane mixtures with silver zeolite A, *J. Am. Chem. Soc.* 134 (2012) 14635–14637.
- [39] J.R. Li, R.J. Kuppler, H.C. Zhou, Selective gas adsorption and separation in metal-organic frameworks, *Chem. Soc. Rev.* 38 (2009) 1477–1504.
- [40] D.M. Ruthven, R.I. Derrah, Transition state theory of zeolitic diffusion. Diffusion of CH₄ and CF₄ in 5A zeolite, *J. Chem. Soc., Faraday Trans. 1: Physical Chemistry in Condensed Phases* 68 (1972) 2332.
- [41] C. Chmelik, J. Kärger, The predictive power of classical transition state theory revealed in diffusion studies with MOF ZIF-8, *Microporous Mesoporous Mater.* 225 (2016) 128–132.
- [42] A. Lauerer, T. Binder, C. Chmelik, E. Miersemann, J. Haase, D.M. Ruthven, J. Karger, Uphill diffusion and overshooting in the adsorption of binary mixtures in nanoporous solids, *Nat. Commun.* 6 (2015) 7697.
- [43] D. Banerjee, S.K. Elsaïdi, P.K. Thallapally, Xe adsorption and separation properties of a series of microporous metal-organic frameworks (MOFs) with V-shaped linkers, *J. Mater. Chem.* 5 (2017) 16611–16615.
- [44] P. Krokidas, S. Moncho, E.N. Brothers, M. Castier, H.K. Jeong, I.G. Economou, On the efficient separation of gas mixtures with the mixed-linker zeolitic-imidazolate framework-7-8, *ACS Appl. Mater. Interfaces* 10 (2018) 39631–39644.
- [45] D.I. Kolokolov, A.G. Stepanov, H. Jobic, Mobility of the 2-methylimidazolate linkers in ZIF-8 probed by ²H NMR: saloon doors for the guests, *J. Phys. Chem. C* 119 (2015) 27512–27520.